

A Broadband Plasmonic Metasurface Superabsorber at Optical Frequencies: Analytical Design Framework and Demonstration

Arvind Nagarajan,* Kumar Vivek, Manav Shah, Venu Gopal Achanta, and Giampiero Gerini

Plasmonic metasurface based superabsorbers exhibit high absorbance. While the absorption peak can be tuned by the geometry/size of the sub-wavelength resonator, broadband absorption can be obtained by harnessing spectrally shifted resonances of multiple resonators of various size/shapes in a unit cell. Metal dispersion hinders high-performance broadband absorption at optical frequencies and careful designing is essential to achieve good structures. A novel analytical framework is proposed for designing a broadband superabsorber which is much faster than the time consuming full-wave simulations that are employed so far. Analytical expressions are derived for the wavelength dependency of the design parameters, which are then used in the optimization of broadband absorption. Numerical simulations report an average polarization-independent absorption of $\approx 97\%$ in the 450–950 nm spectral region with a near unity absorption (99.36%) in the 500–850 nm region. Experimentally, an average absorption over 98% is demonstrated in the 450–950 nm spectral region at 20° incident angle. The designed superabsorber is polarization insensitive and has a weak launch angle dependency. The proposed framework simplifies the design process and provides a quicker optimal solution for high-performance broadband superabsorbers.

in energy harvesting^[1] and high-performance sensing.^[2] A promising pathway to achieve this is to use metasurfaces presenting additional degrees of freedom for tailoring the electromagnetic properties of materials.^[3] Metallic metasurfaces, based on surface plasmon polariton interactions exhibit unique optical properties such as high transmission,^[4] high field concentration,^[5] and perfect absorption.^[6] In the past decade, subwavelength patterned metal–dielectric–metal (MDM) superabsorbers (also termed as perfect absorbers) have been demonstrated to completely absorb the incident light by realizing a perfect impedance matching with free space and by exploiting very high loss guided transmission.^[7–9] Superabsorbers can be classified into narrow-band absorbers^[10] and broadband absorbers^[11–13] depending on the absorption bandwidth. Typically, relative absorption bandwidth ($\Delta f/f_0$) greater than 50% is classified as a broadband absorber.

1. Introduction


Perfect absorption and wave trapping have been major challenges in photonics with numerous potential applications

While narrow-band absorbers are generally used in sensing where strong light–matter interaction is required^[14–18] and absorption filtering,^[19] broadband absorbers find application in thermophotovoltaics^[20] and antireflection surfaces.^[21–24] Broadband absorption is realized by placing multiple resonators in a unit cell and have been demonstrated at various frequencies extending from optical to terahertz range.^[25–34] Specifically, at optical frequencies, Azad et al.^[13] experimentally demonstrated a broadband, polarization independent, wide-angle MDM superabsorber accomplishing more than 90% absorption in the 350–1100 nm spectral region. Alternatively, plasmonic nanocomposites,^[35,36] where Au nanoparticles are randomly dispersed and embedded in a dielectric host offer broadband absorption at optical frequencies. Although, the device fabrication is simpler and do not require e-beam lithography, it is not straightforward to model this system and tune the absorption bandwidth. Vertically aligned single-walled carbon nanotube (SWNT)^[37] also offers ultrabroadband absorption from ultraviolet to far infrared wavelengths. However, the absorption bandwidth of an SWNT cannot be tuned. Si nanowires and nanocone arrays^[38,39] offer theoretical ultrahigh absorbance from ultraviolet to infrared wavelengths. However, the fabrication difficulties limit the practical achievable absorption to $\approx 90\%$. One other approach is to use ultrathin layer of lossy metals like Cr^[40] in an MDM stack. However, the required Cr thickness

A. Nagarajan, K. Vivek,^[†] Prof. G. Gerini
Electromagnetics Group
Technische Universiteit Eindhoven (TU/e)
5600 MB Eindhoven, The Netherlands
E-mail: arvind.nagarajan@tno.nl

A. Nagarajan, K. Vivek, Prof. G. Gerini
Optics Department
Netherlands Organization for Applied Scientific Research (TNO)
Stieltjesweg 1, 2628 CK Delft, The Netherlands

M. Shah, Prof. V. G. Achanta
FOTON Laboratory
Tata Institute of Fundamental Research
Homi Bhabha Road, Mumbai 400005, India

 The ORCID identification number(s) for the author(s) of this article can be found under <https://doi.org/10.1002/adom.201800253>.

^[†]Present address: Development and Engineering, ASML Applications, 5657 EZ Eindhoven, The Netherlands

© 2018 The Authors. Published by WILEY-VCH Verlag GmbH & Co. KGaA, Weinheim. This is an open access article under the terms of the Creative Commons Attribution-NonCommercial License, which permits use, distribution and reproduction in any medium, provided the original work is properly cited and is not used for commercial purposes.

DOI: 10.1002/adom.201800253

is so low (≈ 3 nm) that achieving a uniform layer is difficult. On the other hand, nanopatterned MDM metasurfaces offer the possibility to tailor the design for a specific absorption bandwidth and can be easily fabricated with existing nanolithography techniques. They can also be realized over large areas using nanoimprint lithography.^[41] However, at optical frequencies, the metal dispersion hinders the optimization of resonator dimensions and geometrical features for broadband absorption. Almost all of the previous works on broadband MDM superabsorbers^[11–13,25–34] rely on time consuming full-wave simulations requiring complex optimization routines such as genetic algorithms,^[42] and reported broadband performances at optical frequencies are fewer compared to those at microwave or THz. There is a need for an analytical design methodology to get more insights into the wavelength dependency of the resonator dimensions and other key design parameters, and to allow a better optimization for broadband performance. At the moment, such an analytical methodology has not been reported.

In this paper, we present a novel analytical framework to design and optimize a broadband superabsorber at optical frequencies. The developed analytical framework, uses Gap-plasmon dispersion to get the dimensions of the resonators, and then treats the patterned MDM superabsorber as stacked layers, by homogenizing the array of resonators into an effective medium. The stacked layers are then solved using transfer matrix method. Numerical simulations based on finite element method (FEM) technique test the effectiveness of the proposed framework. The proposed MDM superabsorber is fabricated using electron beam lithography and characterized experimentally.

2. Analytical Framework

A typical MDM superabsorber consists of an array of metal resonators separated from a ground metal plane by a thin dielectric layer. The array of resonators very efficiently couples the incoming light into surface plasmon polaritons (SPPs) at the metal–dielectric interface. The SPPs are then completely dissipated in the structure due to losses, leading to perfect absorption. The resonance can be tuned by modifying the size of the resonators, and broadband performance can be achieved by multiplexing multiple resonators of different shapes in the unit cell. A schematic of a MDM superabsorber is shown in the inset of **Figure 1**. Here, W is the width of the resonator, H is the height, and t_d is the thickness of the dielectric layer. It may be noted that, so far, the optimization of the design parameters for a broadband absorber has been done only numerically, using full-wave simulations. Analytical modeling is restricted to calculating the gap-plasmon dispersion to derive the width of the resonators required to have the resonance at a particular wavelength. In this section, we present a novel analytical framework to design a broadband MDM superabsorber for a general resonator-dielectric-substrate system by computing the required critical design parameters comprising of the resonator width (W) and height (H), and the dielectric thickness (t_d) as a function of operational wavelength (λ). This allows us to optimize the required

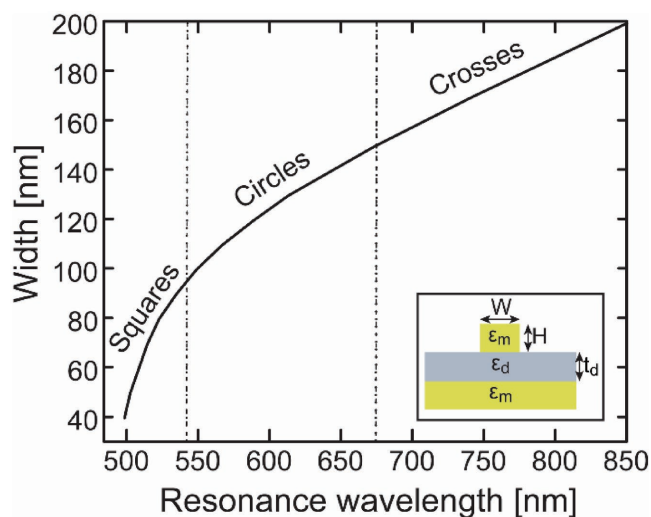


Figure 1. Width (W) of resonator as a function of resonance wavelength (λ) computed by numerically solving the gap plasmon dispersion equation for the metal–dielectric–metal system shown in the inset. The dielectric spacer thickness (t_d) is fixed at 50 nm.

design parameters for broadband absorption in a fully analytical approach.

2.1. Gap Plasmon Dispersion

Metallic nanoparticles have the unique ability of enhancing electromagnetic fields by confining light at subwavelength ranges through the excitation of SPPs at the metal–dielectric interface.^[43] A metal–dielectric–metal system, depicted in the inset of **Figure 1** can be modeled as a continuous layer gap plasmon resonators (CL-GPRs), where the electromagnetic field is localized within the dielectric gap due to magnetic coupling between the SPPs at the two metal–dielectric interfaces. The propagation constant β of the gap-plasmon satisfies the characteristic dispersion equation^[44]

$$\tanh\left(\frac{\sqrt{\beta^2 - k_0^2 \epsilon_d} t_d}{2}\right) = \frac{-\epsilon_d \sqrt{\beta^2 - k_0^2 \epsilon_m}}{\epsilon_m \sqrt{\beta^2 - k_0^2 \epsilon_d}} \quad (1)$$

where k_0 is the wave vector of light in free space; ϵ_m and ϵ_d represent the permittivity for the metal and dielectric. Equation (1) is solved numerically for a dielectric spacer thickness (t_d) of 50 nm (initial guess, which will be refined later). The gap-plasmon effective index (n_{eff}) is given by $\text{Re}(\beta/k_0)$. Finally, the resonator width (W) is computed as a function of resonance wavelength (λ) using Equation (2), where m is the mode index, and ϕ is an additional phase shift

$$W \left(\frac{2\pi}{\lambda}\right) n_{\text{eff}} = m\pi - \phi \quad (2)$$

The Au ground plane is the significant contributor of absorption at lower wavelengths. The phase shift (ϕ) upon reflection from metal is not a straightforward computation. Though for

Table 1. Dimensions of individual resonators used in the design.

Number	Square length (SQ) [nm]	Cylinder diameter (C) [nm]	Cross limb (CR) [nm]
1	40	100	140
2	50	110	160
3	60	120	170
4	70	125	180
5	80	140	190
6	90	150	200

simplicity we assumed it to be zero, in practice, the nonzero phase shift results in a small (≈ 20 nm) redshift of the resonance.^[45] Figure 1 depicts the dependency of the width of the resonators on the resonance wavelength for the fundamental mode ($m = 1$). From Figure 1, 18 resonators with dimensions varying from 40 to 200 nm, in steps of 10 nm, were selected to have a broadband resonance (see Table 1 for dimensions).

2.2. Supercell Design

The gap plasmon dispersion gives only the characteristic width (W) of the resonators, and in principle is the same for any shape of the scattering object such as circles (diameter), squares (side), and crosses (limb). Although a relatively broadband response could be achieved by using only one type of resonator,^[26] a combination of different resonators assists in suppressing the interparticle coupling between two resonators which leads to dips in the absorptions spectrum (see the Supporting Information). The proposed supercell design inspired by recent work^[13] consists of 36 resonators, in a 6×6 grid, with 18 unique resonators consisting of squares (side: 40–90 nm), cylinders^[26] (diameter: 100–150 nm), and crosses^[13,46] (limb; 140–200 nm, width 50 nm) (see Figure 1). The propagation length of SPP in Au is ≈ 20 nm at optical frequencies.^[47] The center to center distance between two adjacent resonators is hence fixed at 250 nm thus guaranteeing a minimum distance between the edges of the elements that allows suppression of coupling between resonators. Polarization independence is achieved by placing the resonators in a fourfold symmetry as shown in Table 2. The periodicity of the supercell is 1500 nm (6×250 nm).

2.3. Effective Medium Approximation

The supercell is then converted into an effective medium such that it can be modeled as a bulk medium of a certain effective

Table 2. Placement of the resonators in the supercell.

SQ1	CR4	C5	SQ4	C4	CR3
CR2	SQ3	C1	CR6	SQ2	SQ6
CR5	C3	SQ5	CR1	C2	C6
C6	C2	CR1	SQ5	C3	CR5
SQ6	SQ2	CR6	C1	SQ3	CR2
CR3	C4	SQ4	C5	CR4	SQ1

permittivity.^[48] This simplifies the MDM superabsorber greatly into a stacked layers structure, and the transfer matrix method (described in the next subsection) can be used to compute the effective resonator height and spacer thickness required for perfect absorption. The asymmetric Bruggeman formulation is used to homogenize the supercell: the effective permittivity ϵ_{eff} is computed at resonance using Equation (3). ϵ_m and ϵ_h are the permittivity of metal and host medium (air), respectively. The fill factor (f) for different resonator shapes is computed using Equation (4), where $L = 1500$ nm denotes the lattice period of the supercell, W is the characteristic width of the resonators, and $W_1 = 50$ nm is the width of the crosses. It is to be noted here that for a given resonance wavelength, the contribution of nonresonating elements in the supercell is negligibly weak and hence they are ignored in the computation of effective permittivity. Figure 2 depicts the computed effective permittivity. The real part of the permittivity is close to 1 (black curve), and the imaginary part of the permittivity (blue curve) is close to zero, confirming the free-space impedance matching

$$\left(\frac{\epsilon_m - \epsilon_{\text{eff}}}{\epsilon_m - \epsilon_h} \right) = (1 - f) \left(\frac{\epsilon_{\text{eff}}}{\epsilon_h} \right)^{\frac{1}{3}} \quad (3)$$

$$f = \begin{cases} 2 \left(\frac{W}{L} \right)^2 & \text{squares} \\ 2\pi \left(\frac{W}{2L} \right)^2 & \text{circles} \\ 2 \left[\left(\frac{2WW_1}{L^2} \right) - \left(\frac{W_1}{L} \right)^2 \right] & \text{crosses} \end{cases} \quad (4)$$

2.4. Transfer Matrix Method

The MDM superabsorber can now be simplified as a stack of two layers of thickness $d_1 = H$ and $d_2 = t_d$ with permittivity ϵ_{eff}

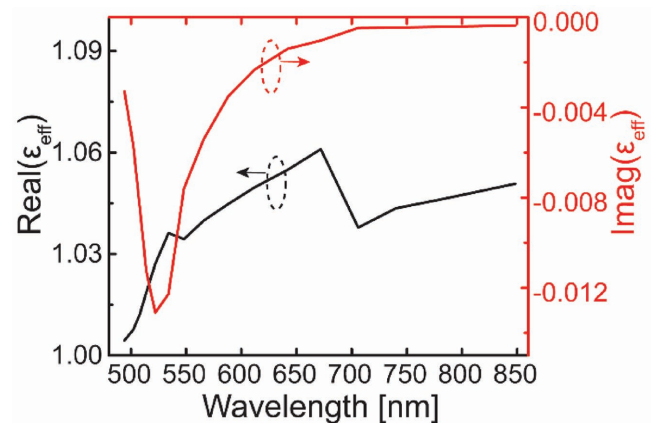


Figure 2. Homogenizing the permittivity of the supercell by asymmetric Bruggeman formulation. The effective permittivity is computed at resonance for each of the resonators. The real part of the effective permittivity is close to 1 (black curve), while the imaginary part is negligibly small (red curve).

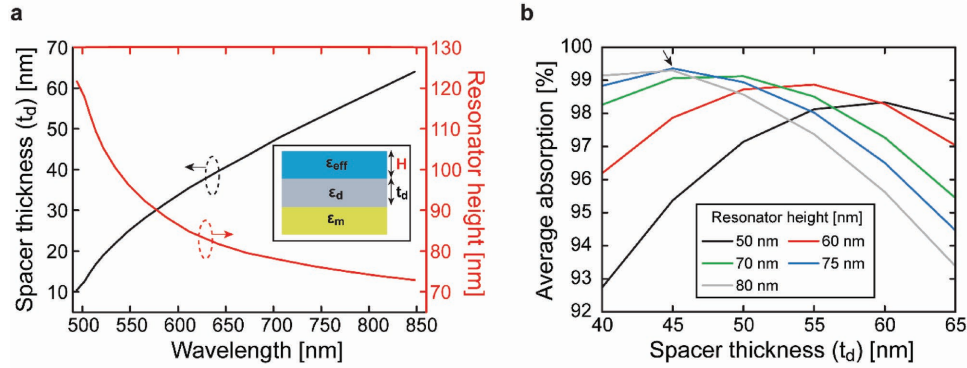


Figure 3. Optimizing the spacer thickness and the resonator height of the supercell. a) Transfer-matrix method results to get the optimal spacer thickness (t_d) (black curve) and the resonator height (H) (red curve) required for perfect absorption at different wavelengths in a 3-layer stack shown in the inset. b) Average absorption of the proposed MDM superabsorber structure in the 500–850 nm spectral range for varying spacer thickness (t_d) and resonator height (H) quantized in steps of 5 nm using full-wave simulations. The arrow indicates the optimal value of 45 and 75 nm for spacer thickness and resonator height, respectively.

and ϵ_d , respectively, embedded between an air superstrate and metal substrate with permittivity ϵ_m (see the inset **Figure 3a**). The relative permeability (μ_r) of the entire system is considered to be 1. Inside the top homogenized layer and the bottom metal layer the waves are evanescent, and hence the wavevectors are purely imaginary, i.e., $k_1 = ik_0\sqrt{\epsilon_{eff}}$ and $k_3 = ik_0\sqrt{-\epsilon_m}$, whereas $k_2 = k_0\sqrt{\epsilon_d}$ is the wavevector in the spacer layer. The transfer matrix (M) for such a system is defined as the product of scattering matrices for each layer (see ref. [45] for derivations)

$$M = \begin{pmatrix} m_{11} & m_{12} \\ m_{21} & m_{22} \end{pmatrix} = S_0 S_1 S_2 S_3 \quad (5)$$

where

$$S_0 = \begin{pmatrix} 1 & 1 \\ k_0 & -k_0 \end{pmatrix}^{-1} \quad (\text{air superstrate}) \quad (6)$$

$$S_j = \begin{pmatrix} \cos(k_j d_j) & \frac{i}{k_j} \sin(k_j d_j) \\ ik_j \sin(k_j d_j) & \cos(k_j d_j) \end{pmatrix} \quad (\text{layers } j = 1, 2) \quad (7)$$

$$S_3 = \begin{pmatrix} 0 & e^{i(d_1+d_2)k_3} \\ 0 & -k_3 e^{i(d_1+d_2)k_3} \end{pmatrix} \quad (\text{metal substrate}) \quad (8)$$

The reflection and transmission amplitudes are given by

$$r = \frac{\gamma_0 m_{11} + \gamma_0 \gamma_3 m_{12} - m_{21} - \gamma_3 m_{22}}{\gamma_0 m_{11} + \gamma_0 \gamma_3 m_{12} + m_{21} + \gamma_3 m_{22}} \quad \text{and} \quad (9)$$

$$t = \frac{2\gamma_0}{\gamma_0 m_{11} + \gamma_0 \gamma_3 m_{12} + m_{21} + \gamma_3 m_{22}}$$

where $\gamma_j = \tilde{n}_j \cos\theta_j$, $\tilde{n}_j = n_j - ik_j$ is the refractive index of j th layer, and θ_j is the angle of incidence. Substituting the S-matrices into M and equating reflection and transmission amplitudes to zero give Equations (10) and (11) for optimal spacer thickness (t_d) and resonator height (H) at normal incidence

$$\cot(k_0\sqrt{\epsilon_d}t_d) = \left(\frac{\sqrt{\frac{-\epsilon_m}{\epsilon_d}} + \sqrt{\frac{\epsilon_d}{\epsilon_{eff}}}}{\sqrt{\frac{-\epsilon_m}{\epsilon_{eff}} - 1}} \right) \quad (10)$$

$$\tan(ik_0\sqrt{\epsilon_{eff}}H) = \sqrt{\frac{\epsilon_{eff}}{-\epsilon_m}} \left(\frac{\sqrt{\frac{-\epsilon_m}{\epsilon_d}} \tan(k_0\sqrt{\epsilon_d}t_d) + 1}{\sqrt{\frac{\epsilon_d}{-\epsilon_m}} \tan(k_0\sqrt{\epsilon_d}t_d) - 1} \right) \quad (11)$$

Figure 3a shows the computed values of the optimal spacer thickness (t_d) (black curve) and the optimal resonator height (H) (blue curve) as a function of resonance wavelength (λ). As seen in Figure 3a, the optimal spacer thickness (t_d) has a nearly linear dependence on the resonance wavelength. The ground Au plane is the significant contributor of absorption at shorter wavelengths. The optimal spacer thickness (t_d) of the supercell is derived as mean from 530–850 nm which gives a value of 42 nm, refining the initial guess of 50 nm. Equation (11) is computed with this value for t_d . The optimal height of the resonators (blue curve) is greater at shorter wavelengths (as can be seen from Figure 3a), but is relatively flat elsewhere. Again, taking into account the significant contribution of ground Au plane in absorption at shorter wavelengths, the height of the resonators is derived as 78 nm (mean from 600–850 nm). Hence, for broadband performance the optimal spacer thickness of the proposed MDM superabsorber is 42 nm, while the optimal height of the resonators in the supercell is 78 nm. Numerical simulations (elaborated in the next section) were performed to test the effectiveness of the proposed framework. The thickness of the spacer layer, and the height of the resonators were swept from 40–65 nm and 50–80 nm, respectively in steps of 5 nm. Figure 3b shows the average absorption at normal incidence obtained in the 500–850 nm spectral range as a function of spacer thickness and resonator height. The absorption is maximum for a spacer thickness (t_d) of 45 nm, and for resonator height (H) of 75 nm, matching quite well with the analytical results.

3. Numerical Simulation

The optical absorption of the proposed MDM superabsorber has been simulated with COMSOL Multiphysics software. The structure consists of 36 Au resonators each of height 75 nm with dimensions given in Table 1, arranged in a 6×6 supercell of periodicity 1500 nm as shown in Table 2. The supercell is separated from the ground Au layer (thickness 200 nm) by a 45 nm SiO₂ layer, and a 5 nm Cr adhesion layer. The edges of the resonators are rounded by 5 nm to account for imperfections in the fabrication. The Johnson and Christy permittivity model^[49] is used for Au and Cr, and Malitson model^[50] is used for SiO₂. In the 3D FEM simulation, Floquet boundary conditions are employed in both x and y directions, and perfectly matched layer boundary conditions are employed in the z direction. The 200 nm thick bottom Au layer is treated as an impedance matching layer (to reduce the computation time, and eliminates the necessity to include the silicon substrate/Cr adhesion layer in the simulation which are essential for device fabrication. This is elaborated in the next section). The absorption is calculated as $A(\lambda) = 1 - R(\lambda)$, where $R(\lambda) = |S_{11}|^2$ is the reflection, as there was no transmission $T(\lambda) = |S_{21}|^2$ in the entire wavelength range.

The simulated normal incidence absorption of the proposed MDM superabsorber structure for both TE (blue curve) and TM (red curve) fundamental modes in the 450–950 nm spectral range is shown in Figure 4. The inset depicts the schematic of the proposed MDM superabsorber. Although the analytical model was designed for the 500–850 nm spectral region, we can observe that the average absorption is above 0.97 for both polarizations in the 450–950 nm spectral region, with near unity absorption between 550 and 850 nm. The ground Au layer accounts for high absorption in the lower wavelength range, and the nonzero phase shift acquired upon reflection from the ground Au layer is attributed to the red shift. The dip ≈ 800 nm in the TE mode is attributed to coupling between Square-4 and Cross-6 (see Figure S3 in the Supporting Information). The

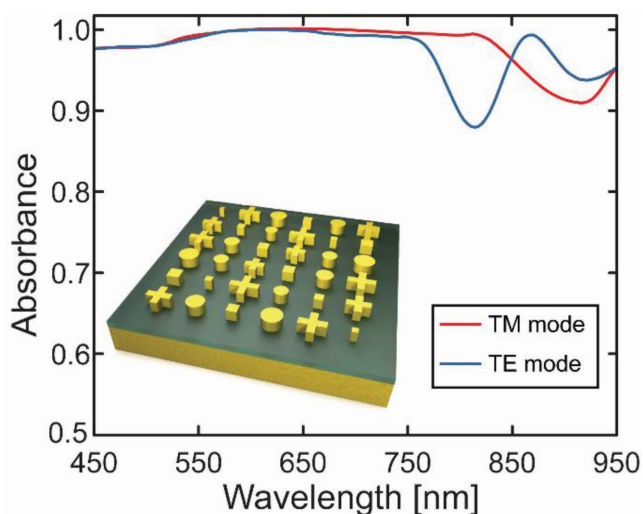


Figure 4. Simulated normal incidence absorption for the TE mode (blue curve) and TM mode (red curve) for the proposed MDM superabsorber structure shown in the inset.

simulated field patterns at various wavelengths are shown in Figure S2 in the Supporting Information.

The angular behavior of the proposed MDM superabsorber is numerically simulated for both polarizations. Figure 5a,b demonstrates that the MDM superabsorber has a weak polarization and launch angle dependence, and has high performance up to 45° (average absorption is 0.896 for TM and 0.943 for TE). The angle dependent absorption of the superabsorber is depicted in Figure 5c,d for both polarizations from 12° to 24° (step size 0.3°). The dispersion is almost flat indicating the absence of grating orders in the 450–950 nm spectral region.

4. Experimental Characterization

The proposed MDM superabsorber structure was fabricated on a silicon substrate using electron beam lithography. The active area of the fabricated device is $300 \mu\text{m} \times 300 \mu\text{m}$. A silicon substrate is chosen to provide the necessary mechanical support. A flexible polymer substrate can also be used.^[51] A 200 nm thick gold film, along with a 5 nm chromium adhesion layer was first deposited on the silicon wafer using DC Magnetron sputtering, followed by chemical vapor deposition of a 45 nm thick SiO₂ film. A 200 nm thick poly-(methyl methacrylate) (PMMA) 459 A4 resist layer was then spin coated. The resist was exposed by an electron beam with 20 kV accelerating voltage and a $10 \mu\text{m}$ focusing aperture. The exposed resist was developed in a 1:3 solution of methyl isobutyl ketone (MIBK) : isopropyl alcohol (IPA) for 90 s and rinsed in IPA for 60 s. A 5 nm chromium adhesion layer and a 75 nm gold layer was then sputtered sequentially on the patterned resist. The resist was later removed by acetone lift-off. A false colored scanning electron microscopy (SEM) image of the sample is shown in Figure 6 (inset).

The polarization and angle dependent reflection of the fabricated sample shown in Figure 6 is measured using a collimated ($<0.3^\circ$ divergence) halogen lamp (450–950 nm) source with $120 \mu\text{m}$ spot and a USB-2000 fiber spectrometer (Ocean Optics). The angle of incidence is limited to 20° – 45° due to mechanical constraints of the setup. Sample reflection spectra were source normalized, from which we derived the sample extinction. As there was no measurable transmittance (see Figure S4 in the Supporting Information) and nonspecular reflection in the entire spectral range studied, it is assumed that the extinction is equal to the absorbance. At 20° incident angle, we report an average absorption of over 98% for both polarizations in the 450–950 nm spectral region. Average absorption measured for various incidence angles match well with simulations, and is tabulated in Table 3. The uncertainty in the reported experimental data is 0.05%. The artefacts/inhomogeneity in the device fabrication, and the possible deviations from the tabulated permittivity of Cr can explain the marginally better experimental performance, and the broadening of the dips in the spectrum (more pronounced at 45°). Device fabrication can further be improved by implementing strategies reported in,^[52] and techniques such as PEEL^[53] (a combination of phase-shifting photolithography, etching, electron-beam deposition and lift-off of the film) and substrate conformal imprint lithography (SCIL)^[54] can be used for large area fabrication. Numerical simulations were carried out to model the effects of inhomogeneity in crosses: all the

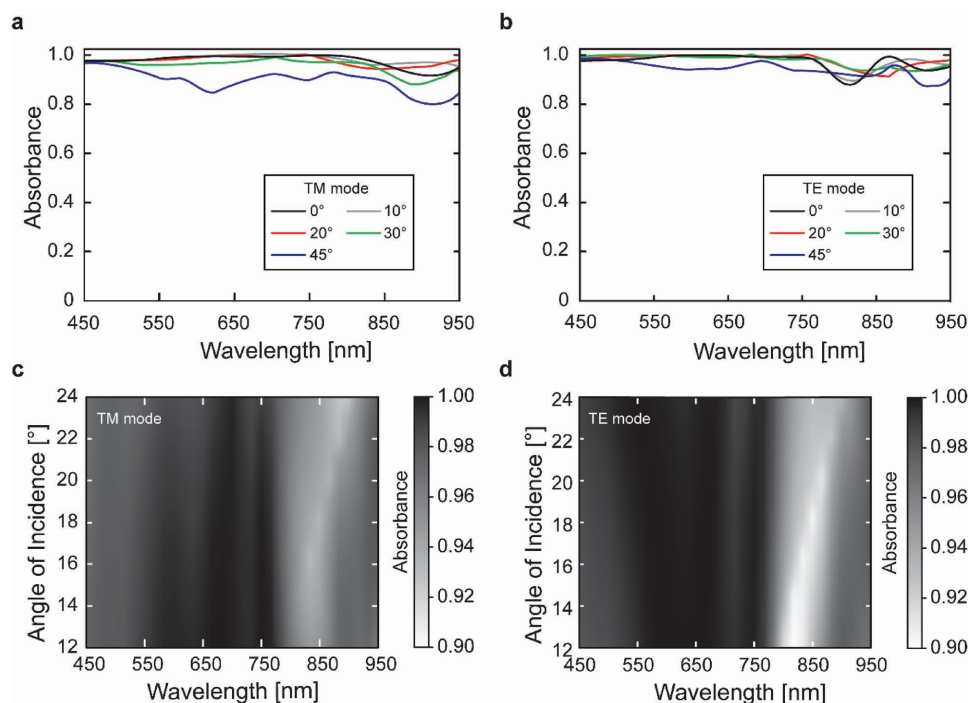


Figure 5. Simulated angle dependent absorption of the proposed MDM superabsorber structure for the a) TM mode and b) TE mode. Dispersion for the TM and TE modes are shown in panels (c) and (d), respectively. The dip in the spectrum centered around 850 nm is the grating order, which becomes more pronounced at higher launch angles.

crosses in the supercell were replaced by diamonds of appropriate dimensions (see Figure S1 in the Supporting Information). Although the experimentally realized crosses have significant inhomogeneity, the experimental response matches better with simulations having crosses rather than diamonds.

5. Conclusions

A novel analytical framework for the design of a broadband, polarization independent superabsorber is presented in this work. The analytical design results are substantiated by

numerical simulation results. We report an average polarization independent absorbance of $\approx 97\%$ in the 450–950 nm bandwidth spanning the entire optical region. Experimentally, an absorbance of over 98% in the 450–950 nm spectral region at 20° launch angle has been demonstrated. These results are in a good agreement with simulations. The presented framework can be applied to design a superabsorber in any wavelength region with any MDM combination. It is particularly useful for dispersive materials. It can be extended for higher angles and higher modes. Although intended for normal incidence and fundamental modes, this framework is the first step in having an all analytical approach to design and optimize the MDM superabsorbers.

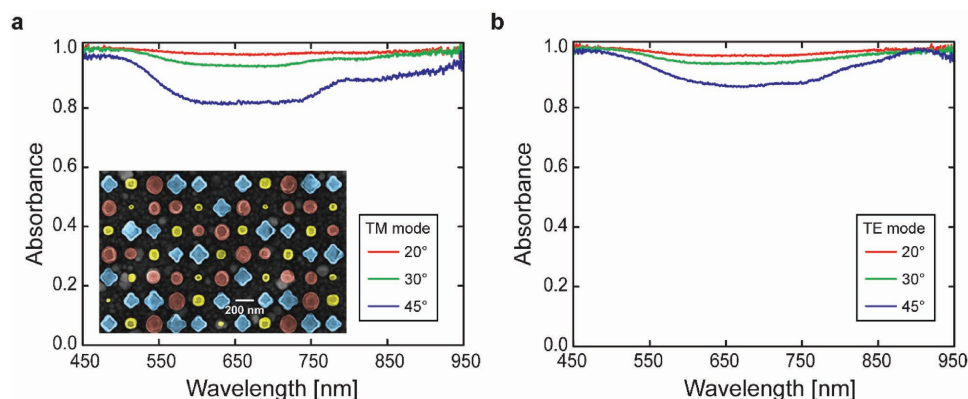


Figure 6. The measured angle dependent absorption $A = 1 - R$ of the fabricated device for the a) TM mode and b) TE mode. The inset shows the false colored SEM image of the fabricated device. Squares, circles, and crosses are coded by yellow, red, and blue, respectively. The white scale bar represents 200 nm.

Table 3. Average absorption in the 450–950 nm spectral range.

Angle of incidence [°]	Numerical simulation		Experiment	
	TM mode	TE mode	TM mode	TE mode
0	97.92%	97.30%	–	–
20	97.64%	97.89%	98.85%	98.60%
30	95.64%	97.67%	96.73%	96.97%
45	89.60%	94.30%	88.30%	92.92%

Supporting Information

Supporting Information is available from the Wiley Online Library or from the author.

Acknowledgements

The authors would like to thank Dr. Man Xu, Dr. Sachin Kasture, and Dr. Benjamin Brenny for discussions and comments on the manuscript. This work was funded by TU/e through the MELISSA PhD project, and by TNO through the Early Research Program (ERP) on “3D Nanomanufacturing”.

Conflict of Interest

The authors declare no conflict of interest.

Keywords

effective permittivity, light confinement, superabsorbers

Received: February 26, 2018

Revised: May 9, 2018

Published online:

- [1] C. Fei Guo, T. Sun, F. Cao, Q. Liu, Z. Ren, *Light Sci. Appl.* **2014**, *3*, e161.
- [2] Y. Long, Y. Li, L. Shen, W. Liang, H. Deng, H. Xu, *J. Phys. D: Appl. Phys.* **2016**, *49*, 32LT01.
- [3] W. Cai, V. Shalaev, *Optical Metamaterials*, Springer, New York **2010**.
- [4] S. Kasture, A. P. Ravishankar, V. J. Yallapragada, R. Patil, N. V. Valappil, G. Mulay, V. G. Achanta, *Sci. Rep.* **2014**, *4*, 5257.
- [5] Z. Yong, S. Zhang, C. Gong, S. He, *Sci. Rep.* **2016**, *6*, 24063.
- [6] N. I. Landy, S. Sajuyigbe, J. J. Mock, D. R. Smith, W. J. Padilla, *Phys. Rev. Lett.* **2008**, *100*, 207402.
- [7] Y. P. Lee, J. Y. Rhee, Y. J. Yoo, K. W. Kim, *Metamaterials for Perfect Absorption*, Springer, Singapore **2016**.
- [8] I. E. Khodasevych, L. Wang, A. Mitchell, G. Rosengarten, *Adv. Opt. Mater.* **2015**, *3*, 852.
- [9] C. Ji, K.-T. Lee, T. Xu, J. Zhou, H. J. Park, L. J. Guo, *Adv. Opt. Mater.* **2017**, *5*, 1700368.
- [10] M. R. S. Dias, C. Gong, Z. A. Benson, M. S. Leite, *Adv. Opt. Mater.* **2018**, *6*, 1700830.
- [11] K. Aydin, V. E. Ferry, R. M. Briggs, H. A. Atwater, *Nat. Commun.* **2011**, *2*, 517.
- [12] J. Zhao, Y. Cheng, *J. Electron. Mater.* **2016**, *45*, 5033.
- [13] A. K. Azad, W. J. M. Kort-Kamp, M. Sykora, N. R. Weisse-Bernstein, T. S. Luk, A. J. Taylor, D. A. R. Dalvit, H.-T. Chen, *Sci. Rep.* **2016**, *6*, 20347.
- [14] N. Liu, M. Mesch, T. Weiss, M. Hentschel, H. Giessen, *Nano Lett.* **2010**, *10*, 2342.
- [15] W. Wu, M. Ren, B. Pi, W. Cai, J. Xu, *Appl. Phys. Lett.* **2016**, *108*, 73106.
- [16] P. Mandal, *Plasmonics* **2016**, *11*, 223.
- [17] K. V. Sreekanth, S. Sreejith, S. Han, A. Mishra, X. Chen, H. Sun, C. T. Lim, R. Singh, *Nat. Commun.* **2018**, *9*, 369.
- [18] L. Cong, S. Tan, R. Yahiaoui, F. Yan, W. Zhang, R. Singh, *Appl. Phys. Lett.* **2015**, *106*, 31107.
- [19] K.-T. Lee, S. Seo, L. J. Guo, *Adv. Opt. Mater.* **2015**, *3*, 347.
- [20] H. A. Atwater, A. Polman, *Nat. Mater.* **2010**, *9*, 865.
- [21] F. De Nicola, P. Hines, M. De Crescenzi, N. Motta, *Carbon* **2016**, *108*, 262.
- [22] K. Han, C.-H. Chang, *Nanomaterials* **2014**, *4*, 87.
- [23] J. Yang, F. Luo, T. S. Kao, X. Li, G. W. Ho, J. Teng, X. Luo, M. Hong, *Light Sci. Appl.* **2014**, *3*, e185.
- [24] A. Patra, A. P. Ravishankar, A. Nagarajan, S. Maurya, V. G. Achanta, *J. Appl. Phys.* **2016**, *119*, 113107.
- [25] F. Dincer, O. Akgol, M. Karaaslan, E. Unal, C. Sabah, *Prog. Electromagn. Res.* **2014**, *144*, 93.
- [26] M. G. Nielsen, A. Pors, O. Albrektsen, S. I. Bozhevolnyi, *Opt. Express* **2012**, *20*, 13311.
- [27] H. Ko, D.-H. Ko, Y. Cho, I. K. Han, *Appl. Phys. A* **2014**, *116*, 857.
- [28] A. Ghobadi, H. Hajian, M. Gokbayrak, S. A. Dereshgi, A. Toprak, B. Butun, E. Ozbay, *Opt. Express* **2017**, *25*, 27624.
- [29] M. Luo, S. Shen, L. Zhou, S. Wu, Y. Zhou, L. Chen, *Opt. Express* **2017**, *25*, 16715.
- [30] X. L. Jia, Q. X. Meng, C. X. Yuan, Z. X. Zhou, X. O. Wang, *Phys. Plasmas* **2016**, *23*, 32103.
- [31] Z. Su, J. Yin, X. Zhao, *Sci. Rep.* **2015**, *5*, 16698.
- [32] X. Liu, C. Lan, B. Li, Q. Zhao, J. Zhou, *Sci. Rep.* **2016**, *6*, 28906.
- [33] Q. Song, W. Zhang, P. C. Wu, W. Zhu, Z. X. Shen, P. H. J. Chong, Q. X. Liang, Z. C. Yang, Y. L. Hao, H. Cai, H. F. Zhou, Y. Gu, G.-Q. Lo, D. P. Tsai, T. Bourouina, Y. Leprince-Wang, A.-Q. Liu, *Adv. Opt. Mater.* **2017**, *5*, 1601103.
- [34] H. Tao, N. I. Landy, C. M. Bingham, X. Zhang, R. D. Averitt, W. J. Padilla, *Opt. Express* **2008**, *16*, 7181.
- [35] J. Y. Lu, A. Raza, S. Noorulla, A. S. Alketbi, N. X. Fang, G. Chen, T. Zhang, *Adv. Opt. Mater.* **2017**, *5*, 1700222.
- [36] K. Takatori, T. Okamoto, K. Ishibashi, *Opt. Express* **2018**, *26*, 1342.
- [37] K. Mizuno, J. Ishii, H. Kishida, Y. Hayamizu, S. Yasuda, D. N. Futaba, M. Yumura, K. Hata, *Proc. Natl. Acad. Sci. USA* **2009**, *106*, 6044.
- [38] Z. Y. Wang, R. J. Zhang, S. Y. Wang, M. Lu, X. Chen, Y. X. Zheng, L. Y. Chen, Z. Ye, C. Z. Wang, K. M. Ho, *Sci. Rep.* **2015**, *5*, 7810.
- [39] J. Zhu, Z. Yu, G. F. Burkhard, C.-M. Hsu, S. T. Connor, Y. Xu, Q. Wang, M. McGehee, S. Fan, Y. Cui, *Nano Lett.* **2009**, *9*, 279.
- [40] Z. Li, E. Palacios, S. Butun, H. Kocer, K. Aydin, *Sci. Rep.* **2015**, *5*, 15137.
- [41] W. Wang, M. Ramezani, A. I. Väkeväinen, P. Törmä, J. G. Rivas, T. W. Odom, *Mater. Today* **2018**, *21*, 303.
- [42] A. R. Conn, N. I. M. Gould, P. Toint, *SIAM J. Numer. Anal.* **1991**, *28*, 545.
- [43] J. A. Schuller, E. S. Barnard, W. Cai, Y. C. Jun, J. S. White, M. L. Brongersma, *Nat. Mater.* **2010**, *9*, 193.
- [44] R. Gordon, A. G. Brolo, *Opt. Express* **2005**, *13*, 1933.
- [45] M. G. Nielsen, D. K. Gramotnev, A. Pors, O. Albrektsen, S. I. Bozhevolnyi, *Opt. Express* **2011**, *19*, 19310.
- [46] X. Liu, T. Tyler, T. Starr, A. F. Starr, N. M. Jokerst, W. J. Padilla, *Phys. Rev. Lett.* **2011**, *107*, 45901.
- [47] S. Maier, *Plasmonics: Fundamentals and Applications*, Springer Science & Business Media, New York **2007**.
- [48] W. M. Merrill, R. E. Diaz, M. M. LoRe, M. C. Squires, N. G. Alexopoulos, *IEEE Trans. Antennas Propag.* **1999**, *47*, 142.
- [49] P. B. Johnson, R. W. Christy, *Phys. Rev. B* **1972**, *6*, 4370.
- [50] I. H. Malitson, *J. Opt. Soc. Am.* **1965**, *55*, 1205.
- [51] S. Walia, C. M. Shah, P. Gutruf, H. Nili, D. R. Chowdhury, W. Withayachumnankul, M. Bhaskaran, S. Sriram, *Appl. Phys. Rev.* **2015**, *2*, 11303.
- [52] R. Patil, S. Lan, A. V. Gopal, *J. Nanophotonics* **2014**, *8*, 83896.
- [53] J. Henzie, M. H. Lee, T. W. Odom, *Nat. Nanotechnol.* **2007**, *2*, 549.
- [54] M. A. Verschuuren, *Ph.D. Thesis*, Utrecht University, Netherlands **1977**.